IEEE Access
Multidisciplinary | Rapid Review | Open Access Journal

Received April 9, 2022, accepted April 30, 2022, date of publication May 5, 2022, date of current version May 12, 2022.

Digital Object Identifier 10.1109/ACCESS.2022.3172314

Detuned Resonant Capacitors Selection for Improved Misalignment Tolerance of LCC-S Compensated Wireless Power Transfer System

WEIJIE LI[1], (Graduate Student Member, IEEE), WEIYAO MEI[1], QUAN YUAN[1], YONGFENG SONG[2], ZHONGHAO DONGYE[1], (Member, IEEE), AND LIJUN DIAO[1], (Senior Member, IEEE)

[1]School of Electrical Engineering, Beijing Jiaotong University, Beijing 100044, China
[2]Locomotive and Car Research Institute, China Academy of Railway Sciences Corporation Ltd., Beijing 100094, China

Corresponding author: Zhonghao Dongye (dyzhh@bjtu.edu.cn)

This work was supported in part by the Science and Technology Research and Development Plan of China National Railway Group Company Ltd., under Grant P2020J023.

ABSTRACT This study proposes a detuned resonant capacitor selection strategy to eliminate the influence of the changed coupling coefficient on the transferred power and efficiency of a wireless power transfer (WPT) system using the LCC-S resonant topology. The output characteristics of the conventional tuned LCC-S system and the novel detuned system are analyzed and compared in detail, the different effects of the detuned parameters on the system output performance are expounded by simulations, and an optimal detuned parameter design process is presented. By adjusting the compensated capacitors on the transmitting side, the output voltage can be constant under varying coupling conditions without changing the switching frequency. Experiments with a 1.5kW power scale were conducted to verify the proposed theoretical analysis. The results show that the fluctuation of the output voltage is restricted to 8.2% in the optimized system when the coupling coefficient changes from 0.18 to 0.38. Under the rated coupling conditions, the experimental results demonstrate that compared with ZPA (88.29%) and ZVS (90.66%), ZCS (91.52%) operating conditions are more suitable for a WPT system equipped with IGBTs to improve the overall efficiency.

INDEX TERMS LCC-S compensation, detuned resonant network, misalignment tolerance, wireless power transfer (WPT), parameter optimization.

I. INTRODUCTION

The concept of wireless power transfer (WPT) was firstly proposed by Nikola Tesla in the 19th century. However, significant advancements and developments in WPT technology have occurred in the last 20 years. Based on the merits of this technology, such as galvanic isolation, weatherproofing, convenience and safety, WPT is expected to replace the traditional plug-in power supply mode to improve the charging process of electrical equipment neat and beautiful. WPT can be used in various power supply applications, such as biomedical implants, portable electronics, unmanned aerial vehicles (UAVs) and electric vehicles (EVs), etc [1]–[5].

The associate editor coordinating the review of this manuscript and approving it for publication was Luyu Zhao.

There are three major implementation ways for WPT, namely electromagnetic radiation WPT, electrically coupled WPT, and magnetically coupled WPT [6]–[9]. Among them, magnetically coupled WPT is an extensively used method, and it can be further divided into magnetically coupled inductive WPT (MCI-WPT) [8] and magnetically coupled resonant WPT (MCR-WPT) [9]. Contrasted with the MCR-WPT system, the MCI-WPT system has a more flexible output capability (from a few W to hundreds of kW) with much higher efficiency. Because of its high applicability and safety, MCI-WPT is the most common choice in WPT system designs. In this paper, MCI-WPT is chosen as the research subject, and it will be regarded as WPT for convenience in the following text.

To improve the power transfer performance of the WPT system, the resonant compensation topology must be

implemented in the primary and secondary side circuits. There are four basic compensation topologies, namely SS, SP, PS, and PP topology, in which ''S'' means the LC series resonant circuit that is composed of coils and compensation capacitors, and ''P'' represents the LC parallel resonant circuit that consists of the same components [10], [11]. SS topology is the most commonly used of these four topologies due to its simple structure, coupling coefficient independently compensated capacitors design, and constant output current characteristic. But its biggest deficiency is when the secondary side circuit shut down suddenly, the current induced in the primary side coils will rush to extremely high as short circuit condition to destroy the primary circuit system, which is dangerous to the charging system and staff nearby [12].

As a result, high-order resonant compensation circuits, such as topologies of LCL-S, double-sided LCL (DS-LCL), LCC-S, and double-sided LCC (DS-LCC), have been proposed to avoid similar situations [11]–[17]. The introduction of high-order compensation circuits broadens the design space for resonant parameters. Existing researches have proposed diverse parameter design approaches for different topologies and applications. Yao *et al.* [12] developed a novel parameter tuning method for DS-LCL compensated circuit, which suppress the majority of high-order harmonics to make the system output current more sinusoidal by using the considerable series-connected inductor on both primary and secondary side. However, the larger the inductance, the bulkier the whole system, which means the fairly low power density in LCL-type WPT systems. Hence, the LCC circuit is more often used in large power applications. In [18], a DS-LCC compensation network working at a constant switching frequency is introduced, and its power devices are operating at zero voltage switching (ZVS) conditions. In [19], a parameter design procedure realizing zero current switching (ZCS) for inverter has been analysed and adopted based on an LCC-SP type WPT system, and the differences in voltampere rating of reactive-compensation elements under ZCS design and zero phase angle (ZPA) condition are compared.

Nonetheless, these proposed methods are all based on the standard resonant conditions of LCC topology and the totally aligned coupling conditions. In practice, misalignment between coupling coils usually is inevitable. And in this case, the power output capability of the WPT system will be decreased. So, it is necessary to investigate a method to alleviate the negative effect on system output caused by misalignments. A basic method is to adjust the output voltage or current by controlling the duty ratio or phase-shift angle of the inverter circuit [20]. However, the upper limit of this method is limited by the peak value of the input DC voltage. Some pieces of literature focus on how to modify the structure design of the coupling coils to improve the system misalignment tolerance. Coil structures that have been proved useful include DD coil, DDQ coil, Tripolar coil, etc [21]–[23]. Another way to solve this problem is to add a DC-DC converter, such as Buck or Boost converter, to regulate the system output within a limited range [24], [25]. But it will complicate the circuit and control design of the whole system.

TABLE 1. Comparison of different regulation methods.

Regulation method	Additional circuit	Control strategy	Receiver side	Regulation range	Practical realization
[20]	No	Simple	Simple	Narrow	Simple
[21]	Additional receiver circuit	Complex	Complex	Narrow	Complex
[25]	DC-DC converter	Complex	Complex	Wide	Complex
[26]	Capacitor arrays & switches	Complex	Complex	Wide	Complex
[27]	Adjustable inductor	Simple	Simple	Wide	Complex
This paper	Capacitor arrays & switches	Simple	Simple	Wide	Complex

Besides, some researchers try to find the proper compensation parameter design to help maintain the output performance stable. In [26], Deng *et al.* let the DS-LCC circuit work at the detuned conditions by changing the parallel compensated capacitors on both sides to deal with the coupling effect problem. But the variable parallel compensated capacitors on the secondary side complicate the resonant network design and enlarge the dimension of the receiving system, which will add additional challenges to the structure design and assembly of the secondary side WPT system. Meanwhile, the variable frequency control also makes the control algorithm complex. According to [27], a novel LCC-S topology with constant current (CC) output characteristic is designed and operates at a detuned condition to improve the system efficiency when coupling coils are misaligned. The application of basic LC series resonant topology on the secondary side avoids the complicated receiving system, but the design of adjustable series compensated inductor makes the manufacture of which difficult. From the research findings mentioned above, it can be found that the slightly detuned resonant system will have better tolerance to changing coupling conditions. Table 1 gives a comprehensive comparison of the advantages and disadvantages of various regulation methods to improve the system output stability under wide coupling changing conditions. And the biggest merit of the method proposed in this article is that there is no complicated adjustable inductor manufacture and no bulky receiver circuit design.

In this paper, a detuned parameter design and selection strategy have been proposed to adapt to the LCC-S compensated WPT system, to improve the stability of the system output voltage when a wide variation of coupling coefficient happens, which could be caused by the axial spacing change or misalignment of the power-transmission coils. The main contributions of this paper can be listed as:

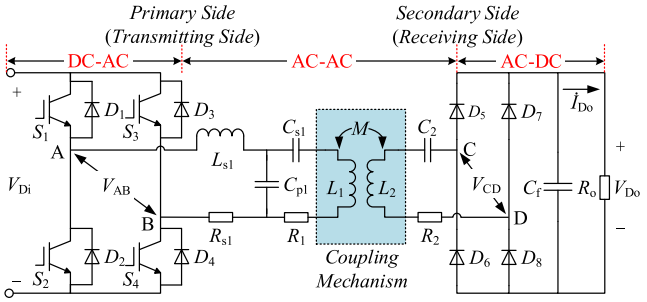

FIGURE 1. Circuit diagram of LCC-S compensated WPT system.

1. Based on the method of fundamental harmonic analysis (FHA) and the T-type equivalent circuit of the LCC-S compensated WPT system, the mathematical models of the conventional tuned LCC-S converter and the detuned one with two variable capacitors on the transmitting side are established, and the corresponding mathematical equations describing their different output characteristics are given and compared.

2. On the basis of the theoretical analysis of the detuned system, the effects of the variable compensation capacitors on the system output voltage gain are illustrated by curve graphs, and it shows that by changing the compensation capacitances on the transmitting side, the output voltage gain could be adjusted dynamically when the coupling conditions of the WPT system changes.

3. According to the derived mathematical equations, a detuned capacitances design and selection scheme is proposed to determine the proper compensation capacitances to help maintain the system output voltage stable under wide coupling changing conditions. The experimental results obtained under detuned and ZCS conditions prove that the adoption of the method proposed can improve the output voltage stability and operating efficiency of the system.

II. THEORETICAL ANALYSIS OF TUNED LCC-S COMPENSATED WPT SYSTEM

The circuit diagram of the LCC-S compensated WPT system is shown in Fig. 1. V_{Di} represents the DC input voltage of the system, V_{AB} is the high-frequency AC square-wave voltage produced by the full-bridge inverter (FBI) composed of IGBT modules ($S_1 - S_4$ and $D_1 - D_4$), V_{CD} is the input voltage of the full-bridge rectifier (FBR) composed by Schottky diodes ($D_5 - D_8$) and V_{Do} indicates the output voltage to supply power to load. L_{s1} is the series-connected resonant compensation inductor on the primary side. C_{s1} and C_{p1} is the series and parallel resonant compensated capacitor on the transmitting side, respectively. C_2 is the series resonant compensation capacitor on the secondary side. L_1 and L_2 represent the transmitting coils and receiving coils, individually. M means the mutual inductance between L_1 and L_2. In addition to these essential resonant components, R_{s1}, R_1, and R_2 are involved in this diagram to represent the equivalent resistance of each loop. C_{f} is the filtering capacitor on the output side, and R_{o} is regarded as the power load.

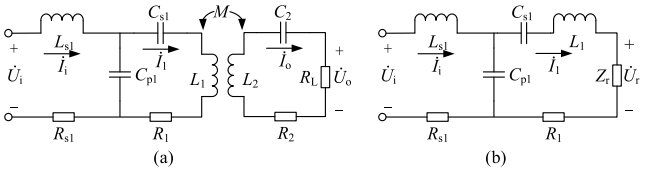

FIGURE 2. (a) Theoretical circuit and (b) T-type equivalent circuit of LCC-S compensated WPT system.

Due to the band-pass effect of the resonant tank, only the fundamental component of the square wave is considered in the theoretical analysis for simplicity [26], [28]. Utilizing the method of FHA, the theoretical circuit model of the LCC-S compensated system can be depicted in Fig. 2(a). In which, $\dot{U}_i$ and $\dot{U}_o$ indicates the input and output voltage of the LCC-S resonant topology, namely V_{AB} and V_{CD}, respectively. And R_{L} denotes the equivalent load resistance, which is made up of the FBR, the output filtering capacitor, and the actual power load.

$$R_L = \frac{8}{\pi^2} R_o \tag{1}$$

According to Kirchhoff's Voltage Law (KVL), the secondary loop voltage equations can be obtained as

$$\begin{cases} j\omega M \dot{I}_1 = \left(R_2 + j\omega L_2 + \dfrac{1}{j\omega C_2} \right) \dot{I}_o + \dot{U}_o \\ \dot{U}_o = R_L \dot{I}_o \end{cases} \tag{2}$$

Thus, the circuit impedance of the receiver side can be calculated as

$$Z_2 = j\omega L_2 + \frac{1}{j\omega C_2} + R_L + R_2. \tag{3}$$

When Z_2 has reflected the transmitting side, the equivalent T-type circuit of LCC-S topology can be obtained as shown in Fig. 2(b).

And the reflected resistor Z_{r} is

$$Z_r = \frac{-j\omega M \dot{I}_o}{\dot{I}_1} = \frac{\omega^2 M^2}{Z_2}. \tag{4}$$

According to the equivalent T-type circuit shown in Fig. 2(b), the equations describing the relationship between the input impedance and input voltage of LCC-S compensation topology can be derived as

$$\begin{cases} Z_{in} = j\omega L_{s1} + R_{s1} \\ \qquad + \left[\dfrac{1}{j\omega C_{p1}} \| \left(\dfrac{1}{j\omega C_{s1}} + j\omega L_1 + R_1 + Z_r \right) \right] \\ \dot{U}_i = Z_{in} \dot{I}_i. \end{cases} \tag{5}$$

In which, the symbol "||" means the corresponding elements are parallel connected in the circuit.

When the standard resonant conditions expressed as (6) are satisfied, the expressions of input impendence, voltage gain, and current gain of tuned LCC-S compensated WPT system

can be derived as (7).

$$\begin{cases} j\omega_0 L_1 + \dfrac{1}{j\omega_0 C_{s1(o)}} + \dfrac{1}{j\omega_0 C_{p1(o)}} = 0 \\ j\omega_0 L_{s1} + \dfrac{1}{j\omega_0 C_{p1(o)}} = 0 \\ j\omega_0 L_2 + \dfrac{1}{j\omega_0 C_2} = 0 \\ \omega_0 = 2\pi f_0. \end{cases} \tag{6}$$

where, ω_0 indicates the resonant angular frequency, and f_0 is the resonant frequency of the LCC-S topology, namely the switching frequency of the FBI, the subscript of "(o)" is used to refer to that the capacitance is for the standard tuned compensation condition.

$$\begin{cases} Z_{in(Tuned)} = \dfrac{\omega_0^2 L_{s1}^2}{\dfrac{\omega_0^2 M^2}{R_2 + R_L} + R_1} + R_{s1} \\ G_{v(Tuned)} = \left|\dfrac{\dot{U}_o}{\dot{U}_i}\right| = \dfrac{\dfrac{\omega_0^2 M L_{s1}}{R_2 + R_L} R_L}{\omega_0^2 L_{s1}^2 + R_{s1}\left(\dfrac{\omega_0^2 M^2}{R_2 + R_L} + R_1\right)} \\ G_{i(Tuned)} = \left|\dfrac{\dot{I}_o}{\dot{I}_i}\right| = \dfrac{\omega_0^2 M L_{s1}}{\left[\omega_0^2 M^2 + R_1 (R_2 + R_L)\right]} \end{cases} \tag{7}$$

$$G_{v(Tuned)} \approx \frac{M}{L_{s1}} \tag{8}$$

$$\begin{aligned} P_{o(Tuned)} &= \frac{\left(G_{v(Tuned)} \cdot \dot{U}_i\right)^2}{R_L} \\ &= \frac{\left(\dfrac{\omega_0^2 M L_{s1}}{R_2 + R_L}\dot{U}_i\right)^2 R_L}{\left[\omega_0^2 L_{s1}^2 + R_{s1}\left(\dfrac{\omega_0^2 M^2}{R_2 + R_L} + R_1\right)\right]^2} \end{aligned} \tag{9}$$

$$\begin{aligned} \eta_{(Tuned)} &= G_{v(Tuned)} \cdot G_{i(Tuned)} \\ &= \frac{\left(\dfrac{\omega_0^2 M L_{s1}}{R_2 + R_L}\right)^2 R_L}{\left(\dfrac{\omega_0^2 M^2}{R_2 + R_L} + R_1\right)\left[\omega_0^2 L_{s1}^2 + R_{s1}\left(\dfrac{\omega_0^2 M^2}{R_2 + R_L} + R_1\right)\right]} \end{aligned} \tag{10}$$

Ignoring the equivalent resistances of R_{s1}, R_1, and R_2, for their fairly small impacts on the voltage gain, the expression of which can be rewritten as (8). Therefore, the output voltage of LCC-S compensation topology can be reckoned as constant under the rated operating condition (mutual-inductance M is fixed at a certain value), with the invariable design of compensation inductor L_{s1}. Based on (7), (9) and (10) can be used to calculate the output power and efficiency of the tuned LCC-S circuit.

III. THEORETICAL ANALYSIS OF DETUNED LCC-S COMPENSATED WPT SYSTEM

In the conventional tuned LCC-S resonant topology, the perfect CV output performance is acquired premising the mutual inductance M is constant under the overall operating conditions. But in practice, the mutual-inductance between the transmitting and receiving coils will change when the misalignment happened or the axial distance of coils varied. According to (8), the variation trend of the voltage gain $G_{v(Tuned)}$ is nearly linear when M changes. Consequently, the WPT system will lose the output characteristic of CV output. To solve this problem, a detuned parameter design method by adjusting the values of compensation capacitances on the primary side is studied in this paper. Firstly, the operating characteristics of the detuned LCC-S compensated topology should be analyzed.

In the detuned situation in this paper, the resonant condition of the transmitting side is no longer valid, but that of the receiving side is still satisfied like

$$\begin{cases} j\omega_0 L_2 + \dfrac{1}{j\omega_0 C_2} = 0 \\ \omega_0 = 2\pi f_0 \end{cases} \tag{11}$$

Simultaneously, the detuned status of the LCC-S system is depicted by introducing the detuned coefficients α and β, in this paper. Only the compensation capacitances on the primary side are changed, and the other resonant parameters maintain unaltered under the detuned situation.

$$\begin{cases} C_{s1(Detuned)} = \alpha \cdot C_{s1(o)} \\ C_{p1(Detuned)} = \beta \cdot C_{p1(o)} \end{cases} \tag{12}$$

Similarly, the expressions of input impedance, voltage gain, and current gain of the detuned system can be derived as

$$\begin{cases} Z_{in(Detuned)} = \dfrac{j\omega_0 L_{s1}}{\beta} \cdot \dfrac{A}{B} + R_{s1} \\ G_{v(Detuned)} = \dfrac{\dfrac{\omega_0^2 M L_{s1}}{R_2 + R_L} R_L}{j\omega_0 L_{s1} \cdot A + \beta R_{s1} \cdot B} \\ G_{i(Detuned)} = \dfrac{\dfrac{\omega_0^2 M L_{s1}}{R_2 + R_L}}{\beta \cdot B} \end{cases} \tag{13}$$

In which, the multinomials A and B can be expressed as (14). As a result, the system output power and efficiency can be calculated by (15) and (16), respectively.

$$\begin{cases} A = (\beta - 1)\left(\dfrac{\omega_0^2 M^2}{R_2 + R_L} + R_1\right) + \dfrac{(\alpha - 1)(\beta - 1)}{\alpha} j\omega_0 L_1 \\ \qquad + \dfrac{(\beta - \alpha - 1)}{\alpha} j\omega_0 L_{s1} \\ B = \dfrac{\omega_0^2 M^2}{R_2 + R_L} + R_1 + \left(1 - \dfrac{1}{\alpha}\right) j\omega_0 L_1 \\ \qquad + \left(\dfrac{1}{\alpha} - \dfrac{1}{\beta}\right) j\omega_0 L_{s1} \end{cases} \tag{14}$$

TABLE 2. Parameter settings for simulation model.

Symbol	Parameter	Value
V_{Di}	DC input voltage	170V
f_0	Resonant frequency	30kHz
L_{s1}	Primary series compensation inductance	36.4μH
$C_{\mathrm{s1(o)}}$	Primary series compensation capacitance	0.27μF
$C_{\mathrm{p1(o)}}$	Primary parallel compensation capacitance	0.8μF
L_1 & L_2	Self-inductance of coils	140μH
M	Mutual-inductance between coils	24~36μH
k	Coupling coefficient	0.18~0.26
C_2	Secondary series compensation capacitance	0.2μF
V_{Do}	DC output voltage	170V
R_{L}	Equivalent resistive power load	16Ω
R_{o}	Actual resistive power load	20Ω

$$P_{o(Detuned)} = \frac{\left(G_{v(Detuned)} \cdot \dot{U}_i\right)^2}{R_{L(opt)}} \tag{15}$$

$$\eta_{(Detuned)} = G_{v(Detuned)} \cdot G_{i(Detuned)} \tag{16}$$

To show directly the influence of α and β on the output characteristics of the WPT system, a mathematical model is established in MATLAB. Table 2 lists the parameters used in this model. The coupling coefficient k is used to represent the coupling condition of the power-transferring coils system here. Its rated value is 0.26 ($M = 35\mu$H and $G_{\mathrm{v(Rated)}} = 1.0$) under the standard aligned condition, and the calculating method of k is given as

$$k = \frac{M}{\sqrt{L_1 L_2}}. \tag{17}$$

Take coefficients α and β as the independent variable individually, their different effect on the output voltage gain $G_{\mathrm{v(Detuned)}}$ can be illustrated in Fig. 3 and Fig. 4. Considering the convenience for assembly and adjustment, the variation range of detuned parameters is not larger than 2.

According to the variation trend under detuned operating conditions of the LCC-S compensated system, the following conclusions could be summarized:

1. In Fig. 3(a) and Fig. 4(a), when $\beta < 1.0$, $G_{\mathrm{v(Detuned)}}$ will decrease as α increases, and when $\beta > 1.0$, $G_{\mathrm{v(Detuned)}}$ will increase as α increases.

2. In Fig. 3(b) and Fig. 4(b), when β increases, the increasing rate of $G_{\mathrm{v(Detuned)}}$ will be reduced gradually as α decreases.

3. In Fig. 3(a) and Fig. 4(a), when $\alpha = 1 - L_{\mathrm{s1}}/L_1$ (namely 0.74 in the simulation case), no matter how to alter the value of β, the voltage gain keeps stable as M/L_{s1}. It can be testified by introducing this equation into (13) and (14) and ignoring the effects of equivalent resistances. Consequently, the voltage gain can be expressed as

$$G_{v(Detuned)} \approx \frac{\omega_0 M}{\omega_0 L_{s1} + j\left(\beta - 1\right)\dfrac{\omega_0^2 M^2}{R_L}}. \tag{18}$$

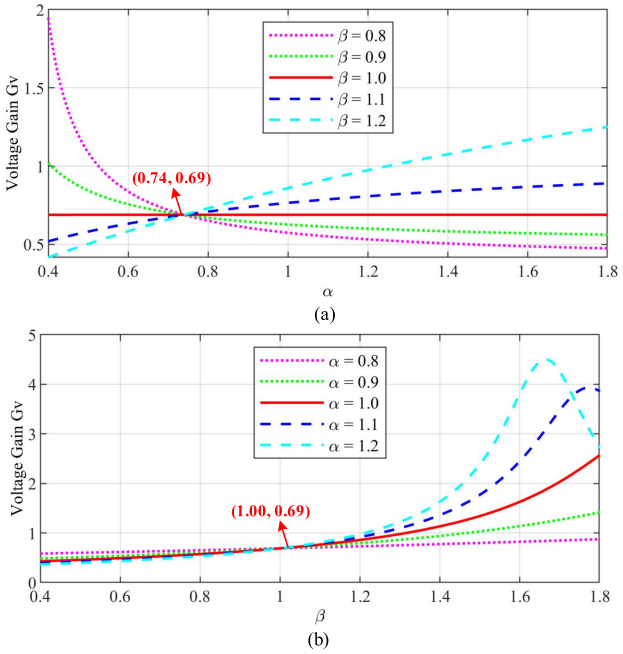

FIGURE 3. When $k = 0.18$, voltage gain changes with (a).

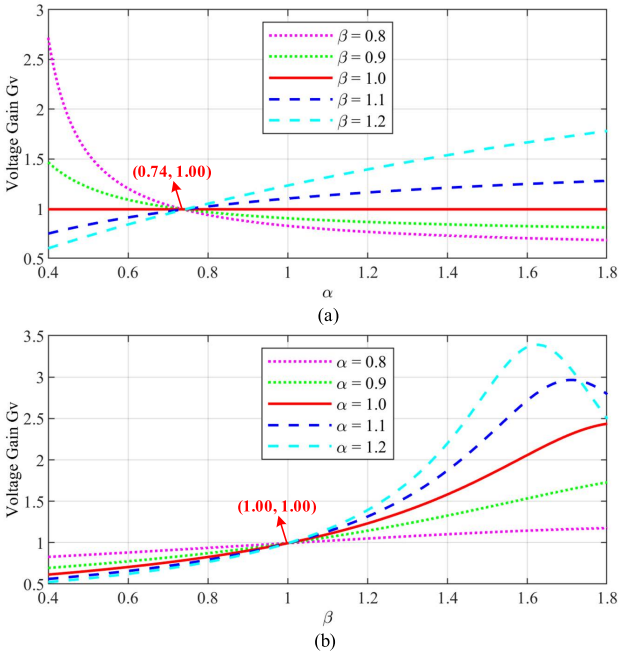

FIGURE 4. When $k = 0.26$, voltage gain changes with (a).

Under the simulation conditions in this paper, the imaginary part of the denominator is much smaller than the real part of that. Thus, (18) will be simplified as (8), to obtain the stable voltage gain independent of parameter β.

4. In Fig. 3(b) and Fig. 4(b), when $\beta = 1.0$, no matter how to alter the value of α, the voltage gain keeps stable as M/L_{s1}. It can be verified by substituting this equation into (13) and (14) and ignoring the effects of equivalent resistances.

As a consequence, the system voltage gain can be depicted approximately as (8) too.

Therefore, it is possible to let the detuned LCC-S system regain the CV characteristic by applying proper combinations of α and β. This mathematical relationship can be described as

$$G_{v(Detuned)}(\alpha, \beta) = G_{v(Tuned)} = G_{v(Rated)}. \tag{19}$$

whereas, there may be different sets of parameter designs that can satisfy the desired output voltage gain for a detuned system. So, it is not sufficient merely by utilizing (19) to determine a set of suitable parameters to get the CV performance of the WPT system. Another restrictive condition should be added to limit the selection of the detuned coefficients further.

IV. REALIZATION CONDITIONS OF DIFFERENT SPECIFIC OPERATING STATUSES FOR THE FBI

According to existing research, the FBI circuit has three major specific operating conditions, namely ZPA, ZVS, and ZCS. In this section, the differences between the three working statuses and their individual realization conditions will be thoroughly examined.

A. ANALYSIS OF THE REALIZATION OF ZPA

The FBI will operate at the ZPA condition when the system input impedance is purely resistive. At the moment, the phase angle between the input voltage and current of the resonant network (i.e. output voltage and current of the FBI) will be zero. On account of the filter effect resulting from the compensation topology, the high-order harmonic components usually will be ignored when calculating the input impedance of the WPT system. Thus, the realization of the ZPA condition is also mainly considering the fundamental component of the input impedance of the resonant compensation network. Based on the results derived from FHA, the system input impedance $Z_{\text{in(Detuned)}}$ under the detuned status can be regarded as shown in (13).

In order to make the input impedance purely resistive, the imaginary part of $Z_{\text{in(Detuned)}}$ should be adjusted to zero. Namely, the restrictive condition for detuned LCC-S compensated WPT system under ZPA operating condition is described as

$$Im\left[Z_{in(Detuned)}(\alpha, \beta)\right] = 0. \tag{20}$$

B. ANALYSIS OF THE REALIZATION OF ZVS

The ZVS design has been widely used in many existing pieces of research and applications to reduce the switching losses of the FBI [26]. Its principle is letting the anti-paralleled diode conduct before the corresponding power device (IGBT or MOSFET) so that the voltage stress across the power device will close to zero when it is switching on. The key point to a successful ZVS implementation is to let the output parasitic capacitor of the power switch be fully discharged within the dead time. Hence, the turn-off current of the power device should be large enough to release the stored power during the limited time:

$$\left|\dot{I}_{off(Detuned)}\right| \geq \frac{4C_{oss}V_{Di,\max}}{t_D}. \tag{21}$$

where C_{oss} is the output capacitance of the power device, and it can be deduced from the datasheet of the power switch easily. t_{D} means the dead time.

To calculate the turn-off current accurately, the higher harmonics of system input power should not be ignored anymore. Applicating the Fourier analysis, the input voltage of the resonant network could be decomposed as:

$$\dot{U}_i = \frac{4}{\pi}\dot{V}_{Di}\sum_{n=1,3,5,\ldots}^{\infty}\frac{\sin(n\omega_0 t)}{n}. \tag{22}$$

The following describes the fundamental input impedance of the LCC-S system in a detuned state.

$$\dot{Z}_{in\_1st} = Z_{in(Detuned)} \tag{23}$$

Meanwhile, the higher harmonic input impedance of the LCC-S resonant topology can be approximately expressed as:

$$\dot{Z}_{in\_nth} \approx R_{s1} + \left(n - \frac{1}{n\beta}\right)j\omega_0 L_{s1}. \tag{24}$$

Therefore, the corresponding fundamental and higher harmonic input current of the resonant network could be derived as:

$$\begin{cases} \dot{I}_{off\_1st(Detuned)} = \dfrac{\dot{U}_{i\_1st}}{\dot{Z}_{in\_1st}} \\ \dot{I}_{off\_nth(Detuned)} = \dfrac{\dot{U}_{i\_nth}}{\dot{Z}_{in\_nth}}. \end{cases} \tag{25}$$

And the calculating expression of the turn-off current is further deduced as:

$$\dot{I}_{off(Detuned)} = \left(\dot{I}_{off\_1st(Detuned)} + \sum_{n=3,5,7,\ldots}^{\infty}\dot{I}_{off\_nth(Detuned)}\right)\Bigg|_{(\omega_0 t=\pi)} \tag{26}$$

On the other hand, the larger the turn-off current is, the higher the turn-off loss of the switching device will be, resulting in lower system efficiency. Consequently, the restrictive condition for detuned LCC-S compensated WPT system under ZVS operating condition is selected as

$$\left|\dot{I}_{off(Detuned)}(\alpha, \beta)\right| = \frac{4C_{oss}V_{Di,\max}}{t_D} \tag{27}$$

C. ANALYSIS OF THE REALIZATION OF ZCS

In [19], the parameter design method for the ZCS operating condition of the LCC type compensated system is proposed. Same with ZVS, the implementation of ZCS is also needed to make the turn-off current satisfy a specific value. But the turn-off current must be equal to zero to achieve the most perfect ZCS operating performance. This means only one set of parameter combinations can make the turn-off current to be zero, and a small but nonzero value of the turn-off current

TABLE 3. Contrast between IGBT and MOSFET.

Comparative item	IGBT (Si)	MOSFET (Si)	MOSFET (SiC)
Maximum of withstand voltage	~6500V	~950V	~1700V
Maximum switching frequency	Tens of kHz	Hundreds of kHz	A few MHz [31]
Tail current	Yes	No	No
Preferable operating condition	ZCS	ZVS	ZVS

will exist under other parameter designs [19]. So, the restrictive condition for detuned LCC-S compensated WPT system under ZCS operating condition can be briefly described as

$$\left|\dot{I}_{off\,(Detuned)}\,(\alpha,\beta)\right| = 0. \tag{28}$$

D. CONTRAST BETWEEN IGBT AND MOSFET ON SWITCHING CHARACTERISTIC

The calculation formula of switching loss of power device is as (29) shows. In which, E_{on} and E_{off} represent the dissipated energy at the moment of the power device turning on and off, respectively. And f_{sw} is the switching frequency of the power device, which equals the resonant frequency of the WPT system. From (29), it can be derived that the switching power loss could be reduced by decreasing either E_{on} or E_{off}, which corresponds to ZVS and ZCS conditions individually.

$$P_{sw-Loss} = \left(E_{on} + E_{off}\right) \cdot f_{sw} \tag{29}$$

For the need for high switching frequency in the WPT system, MOSFET is more often used than IGBT as the power device in the FBI. MOSFET's excellent high-frequency performance allows for very small design values for resonant elements, and existing research has shown that MOSFET is much more suitable to operate at the ZVS condition to reduce switching losses [18], [29]. However, its weakness on withstand voltage limits its application of which on large power-scale occasions. Although the newly developed SiC MOSFET can handle this problem, the cost of that is much higher than the IGBT with the same voltage level.

Unlike MOSFET, IGBT has the tail current to enlarge its turn-off loss when switching off [30]. In consequence, its E_{off} is quite larger than its E_{on}. Theoretically, it is much preferable to let the IGBT operate at the ZCS condition to reduce power loss. Meanwhile, the lower operating frequency of IGBT also helps to cut down the switching loss of which. Despite the design value of the resonant parameters will increase under the lower resonant frequency, it can be acceptable for large power applications. A simple and qualitative contrast between power modules of IGBT and MOSFET can be listed in Table 3.

V. PROPOSED PARAMETER SELECTION STRATEGY

Based on the comprehensive analysis above, two major constraint conditions are presented to direct the optimized parameter design for LCC-S resonant compensation topology to regain the CV performance under detuned operating conditions. For ease of reading and understanding, equations describing the two restrictive conditions in the above content will be reorganized as (30) and (31).

$$F_1(\alpha,\beta) = \mathbf{G}_{v(Detuned)}(\alpha,\beta) = \mathbf{G}_{v(Tuned)} \tag{30}$$

$$F_2(\alpha,\beta) = \begin{cases} Im\left[\mathbf{Z}_{in(Detuned)}(\alpha,\beta)\right] = 0\,(ZPA) \\ \left|\mathbf{I}_{off\,(Detuned)}(\alpha,\ \beta)\right| = \dfrac{4C_{oss}V_{Di,\max}}{t_D}\ (ZVS) \\ \left|\mathbf{I}_{off\,(Detuned)}(\alpha,\ \beta)\right| = 0\,(ZCS) \end{cases} \tag{31}$$

And the implementation process of the proposed parameter selection strategy for coupling changing conditions can be concluded below.

1. Get the rated tuned parameters under standard resonant conditions.
2. Obtain the actual mutual inductance M and coupling coefficient k from the actual G_{v} based on equation (8) when the relative position of power-transferring coils has changed.
3. Take (30) as the first constraint condition of the detuned parameter design guidance, to make the system keep CV output performance when k changes.
4. Select the proper form of (31) as the second constraint condition of the detuned parameter design guidance, to realize specific FBI operating conditions.
5. Solve the equations and get the suitable detuned coefficients α and β.
6. Substitute α and β into the corresponding equations to obtain the optimized value of C_{s1} and C_{p1} for the detuned LCC-S system parameter design.
7. Change the capacitance of C_{s1} and C_{p1} (by switching different capacitor arrays) in the practical WPT system to help the system keep the CV output.

The overall flowchart of this strategy is illustrated in Fig. 5. Although the manufacture of capacitors has around $\pm$ 10% tolerance, and the inductance and capacitance probably have excursions, their influence on detuning parameter regulation is little. Besides, the duty-cycle and phase-shift control could be combined with this detuning method to improve the stability of output voltage further [32], [33].

VI. EXPERIMENTAL VERIFICATION

A. EXPERIMENTAL RESULTS OF TUNED LCC-S SYSTEM

Experiments on a 1.5kW power scale are carried out to validate the feasibility of the proposed parameter design method. Fig. 6 shows the actual experimental setup. The power device composing the FBI is the IGBT module of Infineon FF150R12KT3G, whose operating frequency is 30kHz. The high-frequency rectifier is composed of Schottky Diode of IXYS DSEI2 $\times$ 101. The coupling coils are symmetrical DD-type, and each rectangular coil is wound with 8 turns

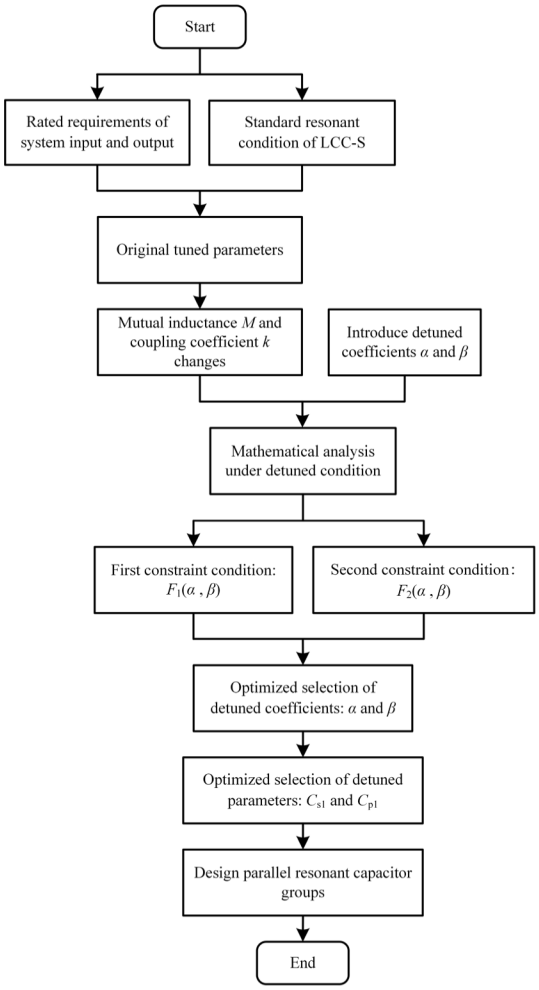

FIGURE 5. Flowchart of the detuned parameter selection strategy.

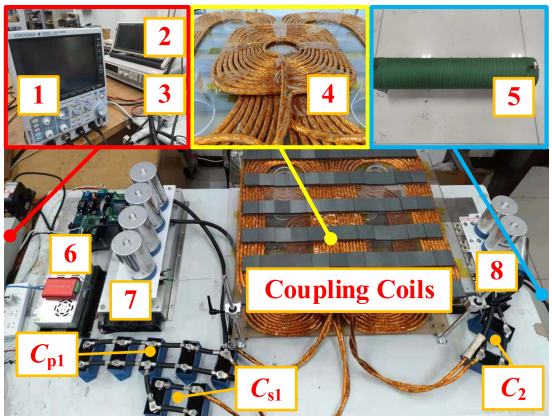

FIGURE 6. WPT experimental platform (1. Oscilloscope, 2. Power analyzer, 3. DC power source, 4. L_{s1}, 5. Resistive load, 6. Control system, 7. FBI, 8. FBR and C_f).

of Litz wire in a single layer. The size of the coupler is 600mm × 600mm. The series compensated inductor L_{s1} is also wound by Litz wire into a rectangle with 12 turns in a single layer, and L_{s1} is overlayed on the transmitting coils

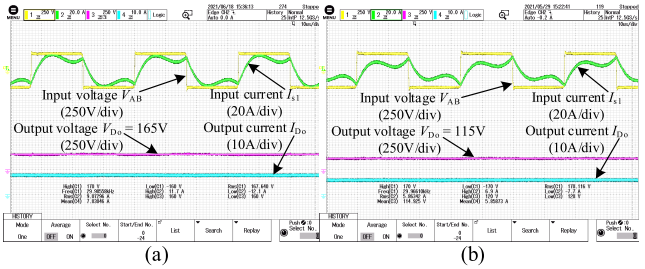

FIGURE 7. Measured waveforms with rated compensation capacitors, when k = (a) 0.26 (ZPA), (b) 0.18.

TABLE 4. Practical experimental conditions.

Parameter	Value	Parameter	Value
V_{Di}	170V	C_{p1}	0.75μF
V_{Do}	170V	L_2	141.24μH
f_{sw}	30kHz	C_2	0.20μF
L_{s1}	37.34μH	M	36.31μH
L_1	140.85μH	k	0.26
C_{s1}	0.27μF	R_o	20Ω

to save space. The size of L_{s1} is 300mm × 300mm. The DC output filter capacitor is 280μF. A resistor with 20Ω is taken as the power load. ITECH IT6513D is the DC power supply with a maximum output capacity of 1.8kW. YOKOGAWA DLM3024 Oscilloscope is utilized to record the experimental waveforms, and HIOKI 3390 Power Analyzer is used to analyze the transferred power and operating efficiency of the whole system.

The rated practical experimental conditions are given in Table 4. And Fig. 7 displays the different output performances of the LCC-S compensated system with the rated compensation capacitors when coupling condition changes. It is clear that as the coupling coefficient k reduces, the output voltage of the conventional tuned system is decreased correspondingly.

B. EXPERIMENTAL RESULTS OF DETUNED LCC-S SYSTEM

Based on the rated compensation capacitances and the detuned parameter selection strategy proposed before, corresponding optimal parameters under different coupling coefficients can be listed in Table 5. In this prototype, the detuned capacitances are realized by different series or parallel combinations of capacitor arrays controlled by off-line switches. Due to the limitation of the capacitances of the actual applied standard capacitors, the optimized resonant capacitances can only be set as close as possible to the ideal calculated ones. And to reduce possible influential factors to verify the effectiveness of the detuned parameters on output regulation, power devices of the FBI are operating with a constant 50% duty ratio, and the closed-loop duty ratio or phase-shift control is not adopted.

Fig. 8–Fig. 10 give the experimental waveforms of the input and output, it can be implied that the CV output and

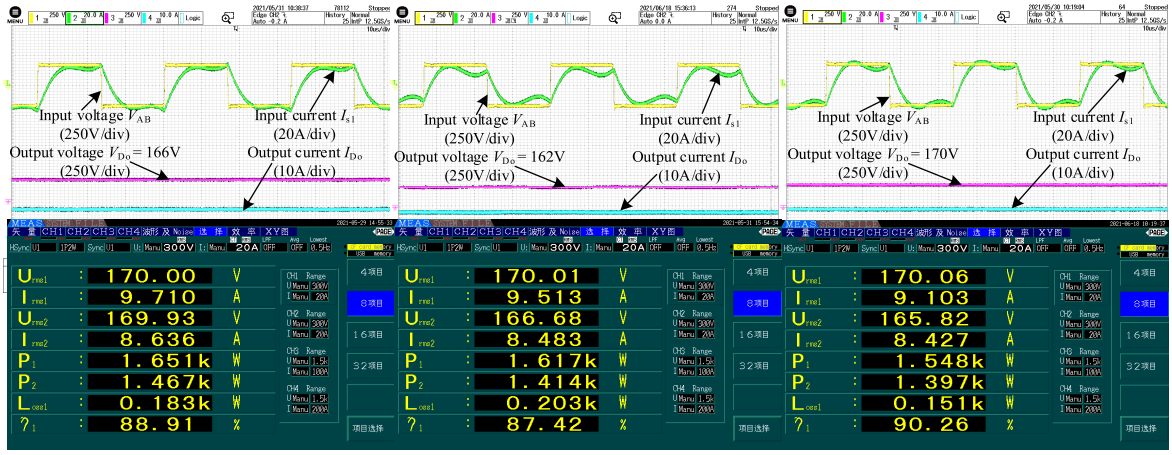

(a) (b) (c)

FIGURE 8. Measured waveforms and efficiency performance of the system with CV and ZPA under k = (a) 0.18, (b) 0.26, (c) 0.38.

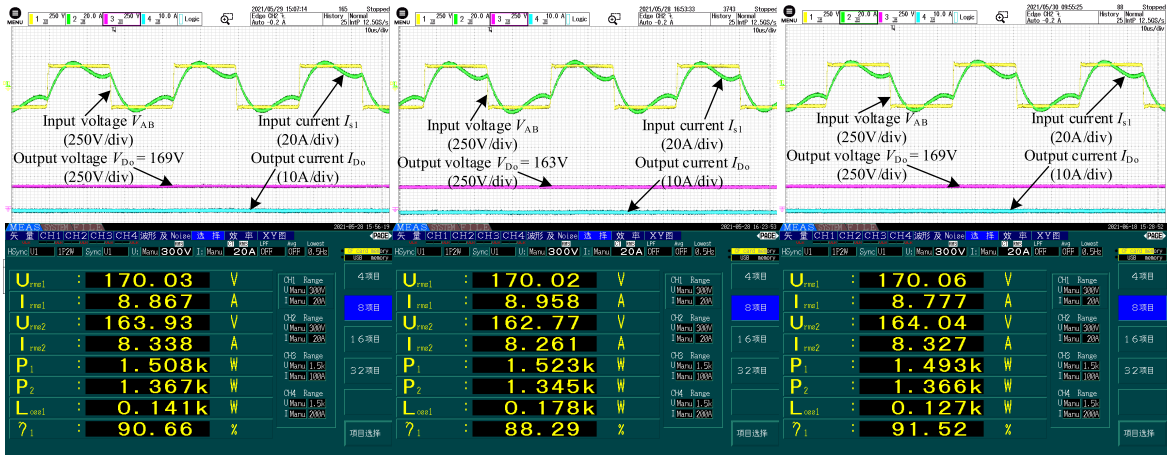

(a) (b) (c)

FIGURE 9. Measured waveforms and efficiency performance of the system with CV and ZVS under k = (a) 0.18, (b) 0.26, (c) 0.38.

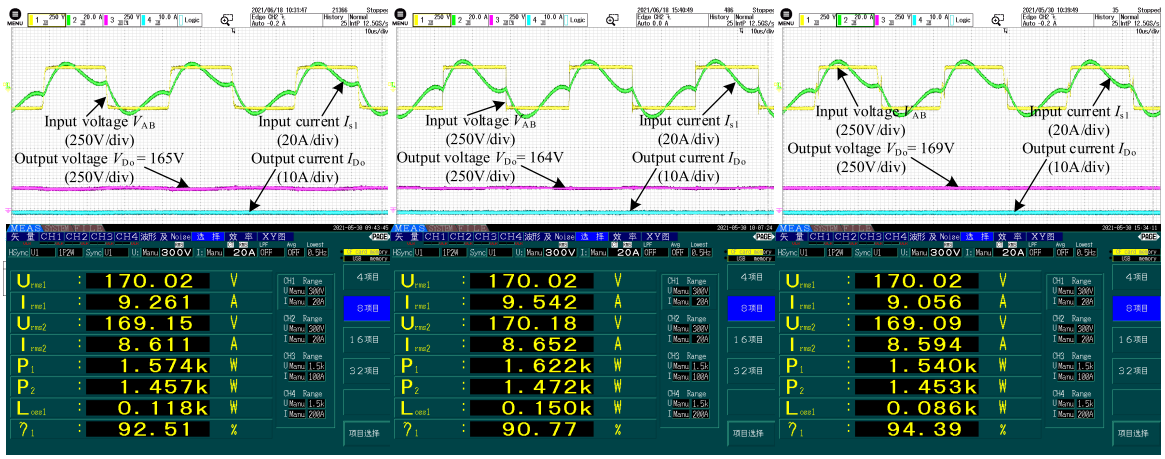

(a) (b) (c)

FIGURE 10. Measured waveforms and efficiency performance of the system with CV and ZCS under k = (a) 0.18, (b) 0.26, (c) 0.38.

different operating conditions (ZPA, ZVS, and ZCS) can be realized by changing the compensation capacitors. The output voltage of the detuned LCC-S WPT system is kept constant at about 170V. Besides, screen captures of the power analyzer

TABLE 5. Optimal parameter designs for different operating conditions.

k	Operating condition	α	$C_{s1(\text{Detuned})}$	β	$C_{p1(\text{Detuned})}$
	ZPA	0.89	0.24μF	1.73	1.30μF
0.18	ZVS	0.93	0.25μF	1.48	1.11μF
	ZCS	0.96	0.26μF	1.51	1.11μF
	ZPA	0.93	0.25μF	1.49	1.12μF
0.21	ZVS	0.96	0.26μF	1.41	1.06μF
	ZCS	1.00	0.27μF	1.37	1.03μF
	ZPA	1.00	0.27μF	1.00	0.75μF
0.26	ZVS	1.04	0.28μF	1.00	0.75μF
	ZCS	1.11	0.30μF	1.04	0.78μF
	ZPA	1.04	0.28μF	0.92	0.69μF
0.30	ZVS	1.04	0.28μF	0.92	0.69μF
	ZCS	1.19	0.32μF	0.91	0.68μF
	ZPA	1.00	0.27μF	0.65	0.49μF
0.38	ZVS	1.11	0.30μF	0.71	0.53μF
	ZCS	1.26	0.34μF	0.75	0.56μF

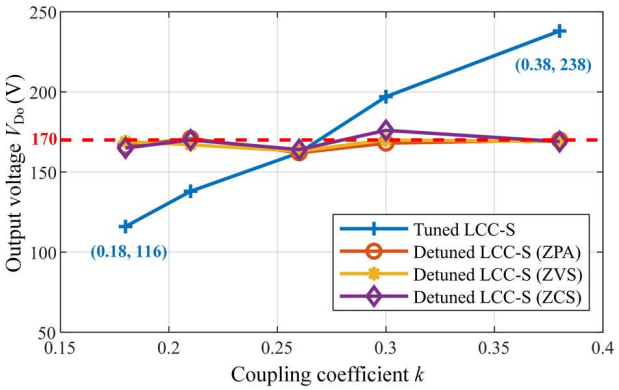

FIGURE 11. Experimental results on output voltage under various coupling conditions.

show the measured system DC-DC efficiencies. Among the measured items displayed in the power analyzer, U_{rms1} and I_{rms1} are system input DC voltage and current, U_{rms2} and I_{rms2} are system output DC voltage and current, P_1 and P_2 are input power and output power of the system individually, L_{oss1} means the power loss of the whole system, and η_1 namely represents the system operating efficiency.

And Fig. 11 compares the output voltages with rated compensated capacitors and variable ones calculated from the proposed method. It is obvious that:

1. The proposed detuned parameter design has a distinct advantage in maintaining the WPT system's CV output characteristic.

2. The output voltage of the tuned WPT system decreases from 238V to 116V when k drops from 0.38 to 0.18. The output voltages of the detuned system with variable compensated capacitors, on the other hand, remain nearly constant.

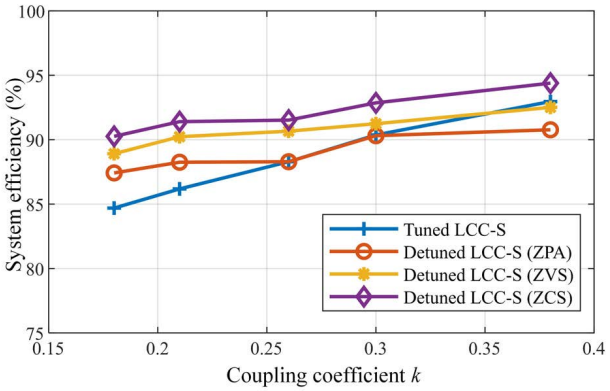

FIGURE 12. Experimental results on system efficiency under various coupling conditions.

Based on the data acquired from the power analyzer, Fig. 12 gives the whole variant trend of system DC-DC efficiency, under different coupling coefficient conditions:

1. When k decreases from 0.38 to 0.18, the system efficiency of the conventional tuned LCC-S WPT system varies from 92.96% to 84.69%. While the efficiency variation ranges of the detuned systems with changed capacitances are quite smaller than that of the tuned ones.

2. The overall efficiency of the LCC-S WPT system under the ZCS condition is the highest, followed by the ZVS condition, and the lowest efficiency is obtained under the ZPA condition. This phenomenon proves that properly designed detuning compensation capacitances also can improve the system efficiency performance.

VII. CONCLUSION

This paper provides a detuned resonant capacitors design and selection scheme for LCC-S compensated WPT system to improve its output voltage stability under wide coupling changing conditions. It is found that by adjusting the compensation capacitances on the primary side, the CV performance can be regained, and the power device in the FBI can operate at ZPA, ZVS, and ZCS status individually, at the same time. Experiments are carried out to prove the validity of the proposed detuned parameter selection strategy, with the coupling coefficient varying from 0.18 to 0.38. It is verified that the output voltage of the detuned LCC-S resonant system can be kept stable (fluctuation value is less than 8.2%) when the coupling condition changed.

The variations of corresponding compensation capacitances are realized by different series or parallel connections of capacitor arrays in this paper. In future research, it can be replaced by switch-controlled capacitors to realize the stepless adjustment of capacitances, and the effects of the introduction of which on system efficiency could be studied and analyzed further.

REFERENCES

[1] C. Xiao, D. Cheng, and K. Wei, "An *LCC-C* compensated wireless charging system for implantable cardiac pacemakers: Theory, experiment, and safety evaluation," *IEEE Trans. Power Electron.*, vol. 33, no. 6, pp. 4894–4905, Jun. 2018.

[2] J. C. Lin, "Wireless power transfer for cell phones or other mobile communication devices and biological implications," *IEEE Microw. Mag.*, vol. 14, no. 5, pp. 18–22, Jul./Aug. 2013.
[3] Z. Zhang, H. Pang, A. Georgiadis, and C. Cecati, "Wireless power transfer—An overview," *IEEE Trans. Ind. Electron.*, vol. 66, no. 2, pp. 1044–1058, Feb. 2019.
[4] S. Li and C. C. Mi, "Wireless power transfer for electric vehicle applications," *IEEE J. Emerg. Sel. Topics Power Electron.*, vol. 3, no. 1, pp. 4–17, Mar. 2015.
[5] R. Bosshard, U. Iruretagoyena, and J. W. Kolar, "Comprehensive evaluation of rectangular and double-D coil geometry for 50 kW/85 kHz IPT system," *IEEE J. Emerg. Sel. Topics Power Electron.*, vol. 4, no. 4, pp. 1406–1415, Dec. 2016.
[6] D. Shi, L. Zhang, H. Ma, Z. Wang, Y. Wang, and Z. Cui, "Research on wireless power transmission system between satellites," in *Proc. IEEE Wireless Power Transf. Conf. (WPTC)*, Aveiro, Portugal, May 2016, pp. 1–4.
[7] F. Lu, H. Zhang, H. Hofmann, and C. C. Mi, "An inductive and capacitive combined wireless power transfer system with LC-compensated topology," *IEEE Trans. Power Electron.*, vol. 31, no. 12, pp. 8471–8482, Dec. 2016.
[8] R. Bosshard and J. W. Kolar, "Multi-objective optimization of 50 kW/85 kHz IPT system for public transport," *IEEE J. Emerg. Sel. Topics Power Electron.*, vol. 4, no. 4, pp. 1370–1382, Dec. 2016.
[9] A. Kurs, A. Karalis, R. Moffatt, J. D. Joannopoulos, P. Fisher, and M. Soljačić, "Wireless power transfer via strongly coupled magnetic resonances," *Science*, vol. 317, no. 5834, pp. 83–86, Jul. 2007.
[10] X. Diao, B. Li, Q. Wu, W. Mei, and L. Diao, "Design and optimization of magnetic coupler based on series-series compensation for EV wireless chargers," in *Proc. IEEE 10th Int. Symp. Power Electron. Distrib. Gener. Syst. (PEDG)*, Xi'an, China, Jun. 2019, pp. 37–42.
[11] W. Zhang and C. C. Mi, "Compensation topologies of high-power wireless power transfer systems," *IEEE Trans. Veh. Technol.*, vol. 65, no. 6, pp. 4768–4778, Jul. 2016.
[12] Y. Yao, Y. Wang, X. Liu, F. Lin, and D. Xu, "A novel parameter tuning method for a double-sided LCL compensated WPT system with better comprehensive performance," *IEEE Trans. Power Electron.*, vol. 33, no. 10, pp. 8525–8536, Oct. 2018.
[13] Y. Su, C. Tang, S. Wu, and Y. Sun, "Research of LCL resonant inverter in wireless power transfer system," in *Proc. Int. Conf. Power Syst. Technol.*, Chongqing, China, Oct. 2006, pp. 1–6.
[14] N. Keeling, G. A. Covic, F. Hao, L. George, and J. T. Boys, "Variable tuning in LCL compensated contactless power transfer pickups," in *Proc. IEEE Energy Convers. Congr. Expo.*, San Jose, CA, USA, Sep. 2009, pp. 1826–1832.
[15] X. Hu, Y. Wang, S. Lv, X. Dong, T. Chen, Y. Jiang, and P. Xu, "Discrete time modeling of wireless power transfer system using LCC compensation topology," in *Proc. 10th Int. Conf. Power Electron. ECCE Asia (ICPE-ECCE Asia)*, Busan, South Korea, May 2019, pp. 968–973.
[16] K. Takeda and T. Koseki, "Analytical investigation on asymmetric LCC compensation circuit for trade-off between high efficiency and power," in *Proc. Int. Power Electron. Conf. (IPEC-Niigata -ECCE Asia)*, Niigata, Japan, May 2018, pp. 2309–2316.
[17] A. Ramezani and M. Narimani, "Optimized electric vehicle wireless chargers with reduced output voltage sensitivity to misalignment," *IEEE J. Emerg. Sel. Topics Power Electron.*, vol. 8, no. 4, pp. 3569–3581, Dec. 2020.
[18] S. Li, W. Li, J. Deng, T. D. Nguyen, and C. C. Mi, "A double-sided LCC compensation network and its tuning method for wireless power transfer," *IEEE Trans. Veh. Technol.*, vol. 64, no. 6, pp. 2261–2273, Jun. 2015.
[19] Z. Pantic, S. Bai, and S. M. Lukic, "ZCS LCC-compensated resonant inverter for inductive-power-transfer application," *IEEE Trans. Ind. Electron.*, vol. 58, no. 5, pp. 3500–3510, Aug. 2011.
[20] Y. Wang, F. Lin, S. Yang, P. Cai, and S. Igarashi, "Efficiency optimization of wireless power transfer system with traction motor load for modern tram," in *Proc. IEEE PELS Workshop Emerg. Technol., Wireless Power Transf. (Wow)*, Jun. 2018, pp. 1–5.
[21] M. Budhia, J. T. Boys, G. A. Covic, and C.-Y. Huang, "Development of a single-sided flux magnetic coupler for electric vehicle IPT charging systems," *IEEE Trans. Ind. Electron.*, vol. 60, no. 1, pp. 318–328, Jan. 2013.
[22] A. Zaheer, H. Hao, G. A. Covic, and D. Kacprzak, "Investigation of multiple decoupled coil primary pad topologies in lumped IPT systems for interoperable electric vehicle charging," *IEEE Trans. Power Electron.*, vol. 30, no. 4, pp. 1937–1955, Apr. 2015.
[23] S. Kim, G. A. Covic, and J. T. Boys, "Tripolar pad for inductive power transfer systems for EV charging," *IEEE Trans. Power Electron.*, vol. 32, no. 7, pp. 5045–5057, Jul. 2017.
[24] K. Song, R. Wei, G. Yang, H. Zhang, Z. Li, X. Huang, J. Jiang, C. Zhu, and Z. Du, "Constant current charging and maximum system efficiency tracking for wireless charging systems employing dual-side control," *IEEE Trans. Ind. Appl.*, vol. 56, no. 1, pp. 622–634, Jan. 2020.
[25] Z. Liu, L. Wang, C. Yin, Y. Guo, and C. Tao, "A research on constant voltage output characteristics of wireless power transfer system with a DC-DC converter," in *Proc. IEEE 15th Brazilian Power Electron. Conf. 5th IEEE Southern Power Electron. Conf. (COBEP/SPEC)*, Dec. 2019, pp. 1–4.
[26] J. Deng, Q. Mao, W. Wang, L. Li, Z. Wang, S. Wang, and G. Guidi, "Frequency and parameter combined tuning method of LCC–LCC compensated resonant converter with wide coupling variation for EV wireless charger," *IEEE J. Emerg. Sel. Topics Power Electron.*, vol. 10, no. 1, pp. 956–968, Feb. 2022.
[27] J. Yang, X. Zhang, K. Zhang, X. Cui, C. Jiao, and X. Yang, "Design of LCC-S compensation topology and optimization of misalignment tolerance for inductive power transfer," *IEEE Access*, vol. 8, pp. 191309–191318, 2020.
[28] M. T. Iqbal and A. I. Maswood, "A frequency domain based large and small signal modeling of three phase dual active bridge," in *Proc. 46th Annu. Conf. IEEE Ind. Electron. Soc.*, Oct. 2020, pp. 3421–3426.
[29] R. W. Erickson and D. Maksimovic, *Fundamentals of Power Electronics*, 2nd ed. New York, NY, USA: Academic, 2001.
[30] T. Suwa and S. Hayase, "Investigation of TCAD calibration for saturation and tail current of 6.5 kV IGBTs," in *Proc. Int. Conf. Simul. Semiconductor Processes Devices (SISPAD)*, Sep. 2019, pp. 1–4.
[31] F. Denk, K. Hahre, R. Kling, and W. Heering, "Investigations of SMPD SiC-MOSFET phase-leg modules for MHz inverters," in *Proc. 18th Eur. Conf. Power Electron. Appl. (EPE ECCE Europe)*, Sep. 2016, pp. 1–7.
[32] M. T. Iqbal and A. I. Maswood, "An explicit discrete-time large- and small-signal modeling of the dual active bridge DC–DC converter based on the time scale methodology," *IEEE J. Emerg. Sel. Topics Ind. Electron.*, vol. 2, no. 4, pp. 545–555, Oct. 2021.
[33] M. T. Iqbal, A. I. Maswood, M. Tariq, A. Iqbal, V. Verma, and S. Urooj, "A detailed full-order discrete-time modeling and stability prediction of the single-phase dual active bridge DC-DC converter," *IEEE Access*, vol. 10, pp. 31868–31884, 2022.